Journal of Neurochemistry

JOURNAL OF NEUROCHEMISTRY | 2016 | 138 | 469–478 doi: 10.1111/jnc.13645

ORIGINAL ARTICLE

Probing amyloid-β pathology in transgenic Alzheimer's disease (tgArcSwe) mice using MALDI imaging mass spectrometry

Louise Carlred,*,†,[1] Wojciech Michno,‡,[1] Ibrahim Kaya,‡ Peter Sjövall,*,† Stina Syvänen§ and Jörg Hanrieder‡,¶,**

*SP Technical Research Institute of Sweden, Borås, Sweden

†Department of Physics, Chalmers University of Technology, Gothenburg, Sweden

‡Department of Psychiatry and Neurochemistry, Sahlgrenska Academy at the University of Gothenburg, Mölndal, Sweden

§Department of Public Health and Caring Sciences, Uppsala University, Uppsala, Sweden

¶Department of Chemistry and Chemical Engineering, Chalmers University of Technology, Gothenburg, Sweden

**Department of Molecular Neuroscience, Institute of Neurology, University College London, London, UK

Abstract

The pathological mechanisms underlying Alzheimer's disease (AD) are still not understood. The disease pathology is characterized by the accumulation and aggregation of amyloid-β (Aβ) peptides into extracellular plaques, however the factors that promote neurotoxic Aβ aggregation remain elusive. Imaging mass spectrometry (IMS) is a powerful technique to comprehensively elucidate the spatial distribution patterns of lipids, peptides and proteins in biological tissues. In the present study, matrix-assisted laser desorption/ionization (MALDI) mass spectrometry (MS)-based imaging was used to study Aβ deposition in transgenic mouse brain tissue and to elucidate the plaque-associated chemical microenvironment. The imaging experiments were performed in brain sections of transgenic Alzheimer's disease mice carrying the Arctic and Swedish mutation of amyloid-beta precursor protein (tgArcSwe). Multivariate image analysis was used to interrogate the IMS data for identifying pathologically relevant, anatomical features based on their chemical identity. This include cortical and hippocampal Aβ deposits, whose amyloid peptide content was further verified using immunohistochemistry and laser microdissection followed by MALDI MS analysis. Subsequent statistical analysis on spectral data of regions of interest revealed brain region-specific differences in Aβ peptide aggregation. Moreover, other plaque-associated protein species were identified including macrophage migration inhibitory factor suggesting neuroinflammatory processes and glial cell reactivity to be

Received January 1, 2016; revised manuscript received April 1, 2016; accepted April 22, 2016.

Address correspondence and reprint requests to Jörg Hanrieder, Department of Psychiatry and Neurochemistry, Sahlgrenska Academy at the University of Gothenburg, Mölndal Hospital, House V, Biskopsbogatan 27, SE-43180 Mölndal, Sweden. E-mail: jh@gu.se

[1]These authors contributed equally to this work.

Abbreviations used: Ac, acetone; ACN, acetonitrile; AD, Alzheimer's disease; APP, amyloid-beta precursor protein; AUC, area under curve; Aβ, amyloid beta; BSA, bovine serum albumin; CA1/CA2/CA3, cornum ammunis regions in the hippocampus; cc, corpus callosum; CHCA, α-cyano-4-hydroxycinnamic acid; CSF, cerebral spinal fluid; ctx, cortex; DG, dentate gyrus; EtOH, ethanol; FAD, familial Alzheimer's disease; FA, formic acid; h-FTAA, heptameric formyl thiophene acetic acids; Hipp, hippocampus; Iba1, ionized calcium binding adaptor molecule 1; IHC, immunohistochemistry; IMS, imaging mass spectrometry; ISD, in-source decay; ITO, indium tin oxide; LMPC, laser microdissection and pressure catapulting; LP, linear positive; m/z, mass-to-charge ratio; MALDI, matrix-assisted laser desorption/ionization; MeOH, methanol; MIF, macrophage migration inhibitory factor; MO, somatomotor cortex; MS/MS, tandem mass spectrometry; NDS, normal donkey serum; OCT, optimal cutting temperature; PBS, phosphate-buffered saline; PBST, PBS/0.1% Tween 20; ROI, region of interest; RP, reflector positive mode; RT, room temperature; SAD, sporadic Alzheimer's disease; SAM, statistical analysis of microarray data; SS, somatosensory cortex; T×100, Triton-×100; TFA, trifluoroacetic acid; tgArcSwe, transgenic Arctic and Swedish mutations; Th, thalamus; TIC, total ion current; TOF, time of flight; VL, lateral ventricle.

involved in AD pathology. The presented data further highlight the potential of IMS as a powerful approach in neuropathology.

Keywords: Alzheimers's disease, amyloid-beta plaques, dementia, MALDI imaging mass spectrometry, tgArcSwe.
J. Neurochem. (2016) **138**, 469–478.

Cover Image *for this issue: doi: 10.1111/jnc.13328.*

Alzheimer's disease (AD) is a neurodegenerative disorder that accounts for the majority of dementia cases, affecting close to 50 million people worldwide (Martin Prince *et al.* 2015). Pathologically, AD is characterized by the formation of protein deposits in the brain including intracellular neurofibrillary tangles consisting of hyperphosphorylated tau protein and extracellular senile plaques that consist of aggregated amyloid-β (Aβ) peptide. A wealth of studies implicate a critical role of Aβ aggregation in early AD pathogenesis, however the mechanisms behind Aβ aggregation and toxicity in AD are not completely understood (Hardy and Higgins 1992; Hardy and Selkoe 2002). Past investigations have revealed that certain genetic mutations within genes encoding the Aβ precursor protein (APP) and associated processing enzymes (PSEN1, γ-secretase) give rise to familial AD (FAD) (van Duijn *et al.* 1991), promote formation and aggregation of Aβ peptides. Although familial AD only accounts for ~ 5% of all AD incidents (Ballard *et al.* 2011), the pathology shares characteristics with the far more prominent sporadic (sporadic Alzheimer's disease) variant of the disease. Therefore, transgenic animal models of AD can serve as model systems for more thorough investigations of the aggregation mechanisms *in vivo* (Philipson *et al.* 2010; Schaeffer *et al.* 2011). For example, the Arctic mutation of APP results in AD, and the corresponding Aβ peptides are more prone to form Aβ protofibrils (Nilsberth *et al.* 2001). A mouse model carrying both the Arctic (E693G) and the Swedish (K670M/N671L) mutation displays extensive Aβ deposition with an early onset age of 5–6 months, and is therefore a well-suited model system to study Aβ pathology (Lord *et al.* 2006). Moreover, using advanced chemical imaging techniques, such as imaging mass spectrometry (IMS), allows for *in situ* characterization of the plaque-associated Aβ pathology in these mouse models.

Imaging mass spectrometry is a powerful approach for probing chemical distribution patterns in complex biological tissue samples (Caprioli *et al.* 1997; McDonnell and Heeren 2007; Hanrieder *et al.* 2013). Matrix-assisted laser desorption/ionization (MALDI) mass spectrometry based IMS is well suited for detection of peptides and proteins as well as lipids *in situ* (Caprioli *et al.* 1997; Hanrieder *et al.* 2011a,b). Using MALDI imaging Aβ peptides have previously been successfully detected and localized in transgenic mouse and single AD patient brain sections (Stoeckli *et al.* 2002; Rohner *et al.* 2005; Philipson *et al.* 2012; Kelley *et al.* 2016), thus providing an opportunity to investigate Aβ pathology in AD without using specific labels.

In the present study, we employed MALDI IMS to investigate the chemical architecture of Aβ deposits in brain tissue of transgenic AD mice carrying the Arctic and Swedish (tgArcSwe) mutation. Multivariate statistical analysis was used to interrogate the IMS data set in order to outline the relevant anatomical features. The Aβ peptide pattern in the detected plaques was verified by immunohistochemistry and laser microdissection followed by MALDI MS and MS/MS (tandem mass spectrometry) analysis. Furthermore, statistical analysis was used to investigate region-specific differences in both the Aβ peptide content and other plaque-associated proteins.

Materials and methods

Chemicals and reagents

All chemicals for matrix and solvent preparation were pro-analysis grade and obtained from Sigma-Aldrich (St. Louis, MO, USA). TissueTek optimal cutting temperature compound was purchased from Sakura Finetek (AJ Alphen aan den Rijn, The Netherlands). The ddH_2O was obtained from a milliQ purification system (Millipore Corporation, Merck Millipore, Billerica, MA, USA).

Animals

Transgenic mice (n = 4, 3 male, 1 female), 18 months of age, with the Arctic (E693G) and Swedish (K670N, M671L) mutations (tgArcSwe) of human APP were reared *ad libitum* at the animal facility at Uppsala University under a 12/12-hlight/dark cycle (Lord *et al.* 2006). The animals were anesthetized with isofluran and killed by decapitation. The brains were dissected quickly with 3 min postmortem delay and frozen on dry ice. All animal procedures were approved by an ethical committee and performed in compliance with national and local animal care and use guidelines (DNr #C17/ 14 at Uppsala University).

Frozen tissue sections (12 μm thick; n = 3/animal) were cut in a cryostat microtome (Leica CM 1520, Leica Biosystems, Nussloch, Germany) at −18°C, and collected on special-coated, conducting glass slides (indium tin oxide, Bruker Daltonics, Bremen, Germany) and stored at −80°C.

Sample preparation

Prior to analysis, tissue sections were thawed in a desiccator for 1 h under reduced pressure (SpeedVac, Eppendorf, Hamburg, Germany). For good protein fixation and preservation, as well as removal of salts and lipids, the tissue sections were washed in cold (−20°C) acetone (Ac) and ethanol for 30 s each, followed by

immersion in cold (−20°C) chloroform for 1 min. Cold solvents were used for better fixation, i.e. dehydration and protein precipitation, resulting in improved preservation of tissue integrity (Altelaar *et al.* 2007). The tissue sections were dried for 15 min under reduced pressure in a desiccator. Prior to matrix application, the sections were scanned in a slide scanner (PathScan Enabler IV, Electron Microscopy Sciences, Hatfield, PA, USA). Using an automated nebulizer sprayer (ImagePrep, Bruker Daltonics, Bremen, Germany), a matrix solution with an initial concentration of 10 mg/mL α-cyano-4-hydroxycinnamic acid (CHCA) dissolved in 70% acetonitrile (ACN) and 0.1% trifluoroacetic acid (TFA) was applied onto the tissue section. The 'CHCA default' program was used for matrix application with the following specifications: matrix thickness, incubation and wetness set to default. The application program comprised five phases with a total of approximately 50 spraying cycles and finished at a plateaued sensor signal that increased 1.9 V from offset, indicating total reflection and full matrix coverage respectively. The corresponding final amount of deposited matrix was approximately 250 μg/cm^2.

MALDI imaging

Tissue localization, sequence generation and automatic data acquisition were performed using the FlexImaging software (v 3.0, Bruker Daltonics). MS data were acquired over a mass range of 2–20 kDa using a Bruker UltrafleXtreme MALDI TOF/TOF instrument running in linear positive mode. Whole tissue section images were acquired at 1 kHz laser repetition rate, collecting 1000 shots per spot with a lateral resolution of 50 μm and the laser beam focus set to medium.

Data processing

All spectra were calibrated externally using the batch-processing function in Flex Analysis (v 3.0, Bruker Daltonics). Calibration spectra were obtained from calibrant solution spots (Protein Calibration Mix 1, Bruker Daltonics) that were placed adjacent to the tissue slides.

For image segmentation, the IMS data were evaluated in SciLS (v2014, Bruker Daltonics) using the corresponding pipeline. Regions of interest (ROIs) were identified by bisecting k-mean clustering based image segmentation. The ROIs were correlated with mass to charge (m/z) values using the corresponding function implemented in the SciLS software. Total ion current normalized average spectra of the annotated ROIs were exported as csv file in FlexImaging. This was followed by binning analysis for data reduction. Here, all ROI data were imported into Origin (v. 8.1 OriginLab, Northhampton, MA, USA) and peaks and peak widths were detected on average spectra of each ROI using the implemented peak analyzer function. The determined bin borders for peak integration were exported as tab delimited text file. The bin borders were used for area under curve peak integration within each bin (peak-bin) of all individual ROI average spectra using an in-house developed R script.

Statistical analysis

Peak area values for all ROI were evaluated using the 'Statistical Analysis of Microarray data' (SAM, v.3.0) in Excel (v.2010) (Tusher *et al.* 2001). The SAM tool was originally developed for microarray analysis and allows comprehensive and unbiased analyses of significant differences in abundance levels between two groups. Two-class, paired analysis of data from Aβ deposits and adjacent control areas was performed for the different anatomical regions, including hippocampus (Hipp), somatosensory cortex (SS) and somatomotor cortex (MO). Further statistical analysis of individual proteins and comparisons between the groups were performed with two-tailed, paired *t* test (95% significance level).

Immunohistochemistry

After MALDI analysis, the tissue sections were rinsed in 95% ethanol for 2 min for matrix removal, and stored in phosphate-buffered saline (PBS, 0.01 M pH 7.4, Sigma-Aldrich). The tissue sections were then fixed in Ac for 10 min at −20°C, and washed three times for 5 min in PBS with 0.1% Tween 20 (0.1% v/v), followed by incubation for 1 h at 22°C in blocking solution containing 5% normal donkey serum (NDS, Invitrogen, Thermo Fisher Scientific, Carlsbad, CA, USA), 2% bovine serum albumin (BSA, Sigma-Aldrich) and 0.3% Triton-X100 (TX100, Sigma-Aldrich). Primary and secondary antibodies were diluted in 1% NDS/0.01% BSA/0.3% TX100. Tissue sections were incubated with primary antibodies overnight at 4°C, and for 1 h at 22°C with secondary antibodies. The following primary antibodies were used: Aβ monoclonal antibody specific for the Aβ1-16 epitope (6E10, 1 mg/mL, BioLegend, San Diego, CA, USA), macrophage migration inhibitory factor (MIF) polyclonal antibody (Anti-MIF, 1 mg/mL, Abcam, Cambridge, MA, USA) and ionized calcium-binding adaptor molecule 1 (Iba1) polyclonal antibody (Anti-Iba1, 1 mg/mL, Abcam, Cambridge, MA, USA), all diluted 1 : 500 in 1% NDS/0.01% BSA/0.3% TX100. Goat anti-mouse IgG conjugated to Alexa Fluor 647 (Life Technologies, Carlsbad, CA, USA) was used as secondary antibody for the detection of the Aβ peptide labels, goat anti-rabbit IgG conjugated to Alexa Fluor 488 (Thermo Fisher Scientific) was used as secondary antibody for the MIF labeling and donkey anti-goat IgG conjugated to Alexa Fluor 555 (Thermo Fisher Scientific) was used as secondary antibody for the Iba1 visualization. All secondary antibodies were diluted 1 : 1000 in 1% NDS/0.01% BSA/0.3% TX100 as described earlier. In order to estimate unspecific binding of the secondary antibodies, a negative control was made by incubation of an adjacent tissue section in diluent solution without the primary antibodies. Each incubation step was followed by 3 × 5 min rinse in PBS-T (0.1% v/v). The slides were subsequently mounted with Prolong Gold antifade reagent (Thermo Fisher Scientific) and dried for 2 h at 22°C. Imaging was performed using a wide field microscope (Axio Observer Z1, Zeiss, Jena, Germany).

Laser microdissection and peptide characterization

Laser microdissection and pressure catapulting (LMPC) was performed on consecutive sections adjacent to the immunostained/MALDI IMS-analyzed tissue. These were mounted on 1.0 PEN (polyethylene naphthalate) membrane slides (Zeiss) and stained with fluorescent chemical amyloid staining (heptameric formyl thiophene acetic acids) for visualization of Aβ deposits. The sections were first thawed in a desiccator and fixed with Ac at 22°C for 10 min. After fixation, the tissue was washed once for 10 min in PBS and then directly incubated for 30 min at 22°C with heptameric formyl thiophene acetic acids, diluted to a final concentration of 3 μM in PBS. The sections were washed once in PBS and then twice in

milliQ water, 5 min each, and then dried for 2 h under reduced pressure in a desiccator. Both the histologically identified plaques and adjacent control area were microdissected using a PALM Microbeam LMPC microscope (Zeiss/P.A.L.M. Microlaser Technologies, Bernried, Germany) equipped with a 355-nm pulsed UV laser. The surface areas of the collected regions were recorded, and the total collected areas were calculated using the preinstalled PALM RoboSoftware 4.6 software (Zeiss). In total, an area of 100 000–120 000 μm^2 of amyloid-positive plaques, and an equivalent area of control material were microdissected from five different mouse brain sections and collected in AdhesiveCap 500 opaque tubes (Zeiss). The thickness of the tissue was 12 μm.

Analysis of isolated Aβ plaques by MALDI-TOF MS and MS/MS

The isolated Aβ plaques were subjected to formic acid (FA) extraction. Here, the material was collected from the adhesive caps by the addition of 50 μL 70% FA and incubated at 22°C for 1 h. FA was removed in a Speedvac (ThermoSavant, Thermo Scientific, Waltham, MA, USA) and the sample was reconstituted in 5 μL 20% ACN/0.1% FA. For MALDI analysis, the samples were prepared with the seed layer method (Tusher *et al.* 2001), including pre-spotting of a matrix seed layer (CHCA, 20 mg/mL, 90% Ac, 10% methanol and 0.005% TFA) and subsequent co-application of 1 μL sample mixed with 1 μL matrix (CHCA, 15 mg/mL, 50% ACN/0.1% TFA). MALDI MS was performed using an UltrafleXtreme MALDI TOF/TOF instrument (Bruker Daltonics) operating in reflector positive mode. Data were acquired over a mass range of 600–5000 Da, with 5000 shots at 1 kHz repetition rate and the laser focus set to medium. The spectra were calibrated externally with peptide standard solution (PepCalMix1, Bruker Daltonics) spotted adjacent to the sample spots on the target.

Peptide fragmentation (MS/MS) was performed using post source decay (LIFT mode). Here, precursor ions of interest were selected with the iongate (PCIS) set to ± 0.4% of the m/z of the intact peptide. About 500–1000 shots were collected in precursor mode followed by switching to fragment mode for one-point calibration of the precursor ion and product ion collection with the laser energy increased by 30%. Post LIFT, mother ion suppression was activated and a number of 5000 shots were collected in fragment mode. The individual MSMS spectra were baseline subtracted and peak picked. Peptide identification was performed in two ways: sequence matching and database search using the BioTools software (v. 3.2, Bruker Daltonics). First, peptide sequences were matched to the corresponding APP sequence using the sequence editor tool in BioTools (Fig. S2). Then, database search was performed using the mascot search engine (MS/MS search, Matrix Science, London, UK). The MS/MS spectra were searched toward the Uniprot database containing the mutant human APP sequence (Arc:E693G, Swe: K670M/N671L) using the following search parameters: taxonomy; all, precursor mass ± 100 ppm; fragment mass ± 0.5 Da; no enzyme; no fixed and variable modifications; instrument MALDI TOF PSD.

Results

Imaging MS of amyloid peptides in mouse brain tissue

The acquired image data were investigated using unsupervised multivariate statistics in order to obtain image segmentation of anatomical regions of interest based on their chemical identity. Here, hierarchical clustering analysis (bisecting k-means) was employed using the implemented feature in the SciLs software (v.2014, SciLs GmbH, Bremen, Germany). Image segmentation identified deposit-like structures mainly in the cortex and hippocampus (Fig. 1a and b). The structures were assigned as individual regions of interest (ROI) and correlated with the processed MS data, in order to identify the associated chemical species that allowed image segmentation of the regions. Here, a number of m/z peaks displayed significant correlation with the putative plaques, including mass peaks at m/z 4000–4500 and m/z 6000–6300 (Fig. 1c). Tentative assignment, based on the accurate mass values, identified the peptides around 4 kDa as differently truncated Aβ species (Table 1). The single ion images of the individual Aβ peptides, Aβ1-37, Aβ1-38 and Aβ1-40, showed strong consistent deposit-like distribution patterns throughout different gray matter regions, including the cortical and hippocampal regions (Fig. 1d–f, Fig. S1).

Amyloid peptide identification and validation

To verify the identity of the detected features, immunohistochemistry was performed, using a monoclonal Aβ antibody (Aβ1-16, 6E10) (Fig. 2a-c). The resulting Aβ immunoreactive features displayed co-localization with the corresponding peptide structures in the IMS data (Fig. 2d–f), further confirming the identity of the deposits as aggregates of Aβ peptides.

For further validation of the identity of the Aβ peptides detected by MALDI IMS, individual amyloid-positive stained plaques were isolated from the tissue by LMPC and analyzed by MALDI MS (Fig. 3a and b). The MALDI analysis of the plaque extracts yielded a number of amyloid peptide species, which were identified based on their accurate mass, as well as their MS/MS data (Table 1). Indeed, the identity of several Aβ peptides observed by MALDI IMS, including Aβ1-37, Aβ1-38, Aβ1-40 and Aβ1-42, was confirmed using the MALDI MS (Fig. 3c) and MS/MS (Fig S2). In contrast, no Aβ peptides were detected in the extract from the control area (Fig. S3).

Plaque-related changes in Aβ peptide patterns

In order to investigate possible variations in the Aβ truncation content for different plaques and different brain regions, the MALDI IMS spectral data of individual Aβ deposits and adjacent control areas were evaluated by statistical analysis. First, in order to identify general plaque-associated protein and peptides, IMS data from all Aβ-positive deposits and adjacent control regions, were analyzed irrespective of the brain region using SAM-based two-class paired *t* statistics. This was then followed by analyzing the plaque and control ROI within each of the three brain regions studied, in order to identify brain region-specific changes in plaque chemistry. Statistical analysis was performed using the SAM (statistical analysis of microarrays) approach for unbiased interrogation of the imaging datasets. In SAM, a score is calculated for each

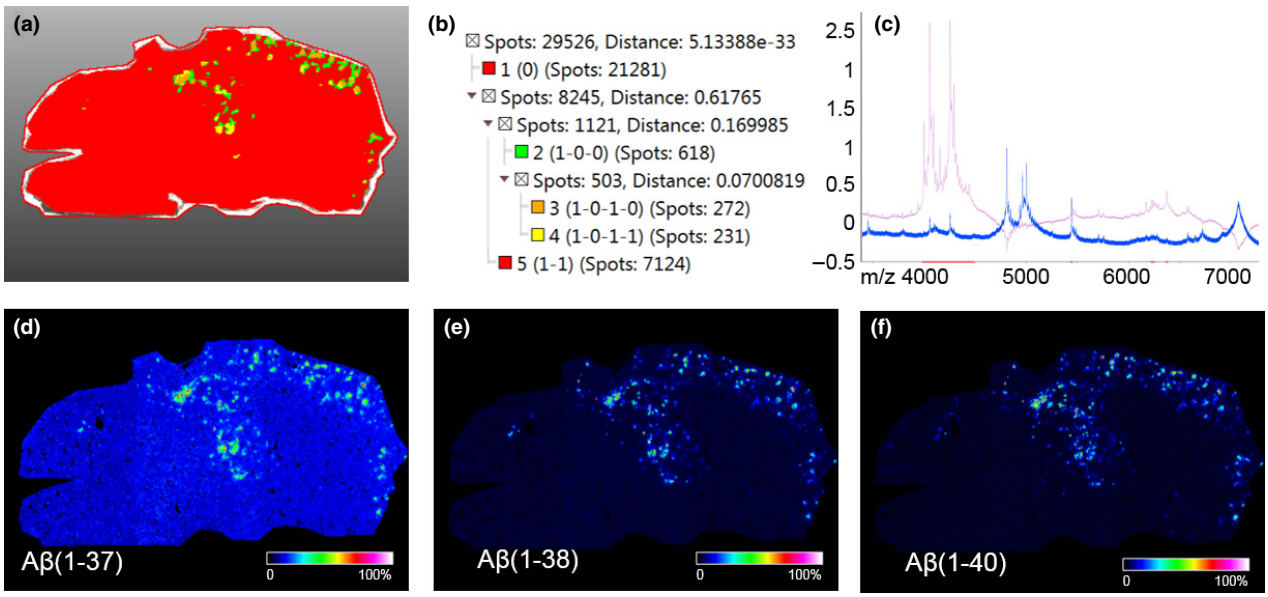

Fig. 1 Matrix-assisted laser desorption/ionization (MALDI) imaging mass spectrometry (IMS) data reveal putative Aβ plaques in the cortical and hippocampal regions of the mouse brain. (a) Segmentation map obtained from multivariate image analysis of MALDI IMS data. (b) Bisecting k-means based clustering analysis identified plaque-like structures (green, yellow, orange) in the cortex and hippocampus (a). The corresponding dendrogram (b) displays the clusters and subclusters (nodes, e.g. 1-0-0), their relation (distance) and the associated number of MS spectra (spots). (c) Correlation of plaque feature data derived MS data (gray) with all acquired MS data (blue) revealed plaque-associated m/z signals (red) including putative Aβ peptides between m/z 4000–4500. (d–f) This is further verified by single ion images of these individual Aβ peptides. Note the distinct Aβ peptide localization patterns resembling plaques.

variable (m/z value) that measures the strength of the relationship between peak intensity and the sample group (i.e. response variable; plaque vs. control). Here, repeated permutations of the data are used in order to determine if the intensity of each variable is significantly different for the two sample groups. The results are presented in plots where the calculated (observed) score is displayed for each variable (m/z value) as a function of the 'expected' score, which is calculated from the fluctuations in the data assuming that there is no difference between the groups. An observed score that is significantly larger than the expected score thus indicates a significant difference between the groups for this variable.

The results show a statistically significant ($p < 0.05$) increase in various signals in all Aβ deposits compared to the control areas (Fig. 4a). Among these signals, the Aβ1-38, Aβ1-40 and Aβ1-42 peptides and a few other truncated forms of the Aβ, which were detected in MALDI IMS, were significantly increased in the plaques as compared to the adjacent control area. Furthermore, region-specific analysis of the hippocampus (Hipp), the somatosensory cortex (SS) and the somatomotor cortex (MO), respectively, showed different localization patterns for the various Aβ peptide species (Fig. 4b–d). Specifically, Aβ1-38 and Aβ1-40 were enriched in the deposits of all brain regions, whereas Aβ1-42 was found to be relatively increased to plaques mainly in hippocampus and somatosensory associated cortex, but not in the somatomotor cortex (Fig. 5).

Plaque-associated protein changes

In addition to Aβ peptides, the SAM analysis of individual Aβ deposits and adjacent control regions did also reveal plaque-associated changes for other proteins. Paired statistical analysis of all deposit and control data, pooled from all brain regions, revealed a number of unknown peptide and protein peaks around m/z 5000–9000 with enhanced signal in the plaques. This included the unknown peaks between m/z 6000–6500, including m/z 6049, 6094, 6109, 6124, 6162, 6175, 6198, 6216, 6234, 6261, 6293, 6371 and 6407. Brain region-specific statistical analysis of deposits and adjacent area revealed differences in between the hippocampus and the cortical areas. In the somatomotor-associated cortex, mass signals at m/z 6049 and 6162 as well as two other unknown signals at m/z 7687 and 9065 were significantly increased in the Aβ plaques as compared to the control area, whereas the other signals showed no significant localization to the plaques. In contrast, the hippocampal region displayed localization of a wide range of signals between m/z 6049-6407 (as described above) and additional unknown signals at m/z 6147, 6277 and 6326 to the deposits.

Among the observed peaks around m/z 6000, one peak at m/z 6175 that was localized to hippocampal plaques (Fig. 6a–c) was putatively attributed to macrophage migration inhibitory factor protein (MIF) based on accurate mass assignment and previously reported MALDI imaging data (Rahman *et al.* 2011). In order to verify the identity and

Table 1 Assignment of observed peaks in tgArcSwe mouse brain tissue using MALDI imaging MS and MALDI MS of extracts from laser microdissected individual plaques respectively

Aβ sequence	Predicted mass (m/z)[a]	MALDI IMS (m/z)	Plaque extract (m/z)
1-42arc Ox[b]	4457.26	4457.11	–
1-42arc	4440.26	4442.01	4440.39
1-42arc Ox $[M+2H]^{2+}$	2228.63	–	2228.58
1-40arc $[M+Na]^{+}$	4279.13	4280.88	–
1-40arc	4256.13	4257.82	4256.23
4-43arc Ox	4242.20	–	4242.21
3-42 pE	4236.19	4236.19	–
1-39arc	4157.07	4157.89	4157.12
2-40arc	4141.11	–	4142.06
5-43 Ox	4095.13	4096.50	–
3-40arc $[M+Na]^{+}$	4093.07	4093.78	–
3-40arc Ox	4086.07	–	4086.07
1-38arc $[M+Na]^{+}$	4081.00	4083.18	–
1-38arc Ox	4074.00	–	4074.11
1-38arc	4058.00	4060.25	4058.10
2-39arc	4042.04	4042.01	4042.08
1-37arc	4000.98	4002.53	4000.97
3-39arc Ox	3987.00	–	3987.07
1-36arc	3943.95	–	3944.19
11-40arc	3078.66	–	3078.91
7-28arc	2434.18	–	2434.45
11-33arc	2423.28	–	2423.76

[a]Predicted mass corresponds to the singly charged species $[M+H]^{+}$ based on the theoretical molecular mass of the corresponding Aβ peptide, if not specified otherwise (e.g. $[M+Na]^{+}$ or $[M+2H]^{2+}$).
[b]Ox refers to oxidation (M+16).

degree of localization of the detected putative MIF signal, immunohistochemistry was performed towards Aβ(1–16) (Fig. 6d), macrophage migration inhibitory factor (MIF) (Fig. 6e) as well as for ionized calcium binding adaptor molecule 1 (Iba1), a marker for activated microglia (Fig. 6f). Indeed, the immunostaining revealed a high degree of co-localization of MIF and activated microglia (Iba1) to the Aβ-positive deposits in the hippocampal region (Fig. 6g). This further confirmed the identity and localization of MIF in the plaques proximity as well as further supports its relevance in plaque pathology-associated microglial activation.

Discussion

Extracellular deposits, or plaques, consisting of aggregated Aβ peptides are considered the main pathological hallmark of Alzheimer's disease (AD). While this amyloid pathology has been suggested to be a critical inducer of AD pathogenesis, no direct correlation has been found between the plaque burden and AD progression (Arriagada *et al.* 1992). Instead, formation of Aβ plaques in specific brain regions has been considered a key element in neuropathological staging of AD (Braak and Braak 1991). Previously, a wide variety of different Aβ peptides have been reported to be present and differently distributed not only in brain tissue of both the sporadic and familial (FAD) cases of the disease, but also specifically in mouse brains with the tgArcSwe mutation (Tekirian 2001; Philipson *et al.* 2009; Portelius *et al.* 2010; Lillehaug *et al.* 2014). In these studies, immunoprecipitation (IP) on brain tissue homogenates and ELISA assays and/or MALDI MS was shown to be a reliable method for Aβ peptide detection and quantification. However, as for all work on tissue extracts, the spatial information of peptide changes is not obtainable.

Here, we employed MALDI imaging mass spectrometry (IMS) to identify and characterize deposit-like structures in the cortex and hippocampus of tgArcSwe mouse brains. We demonstrate that MALDI IMS is able to detect different Aβ peptide species directly *in situ* (Fig. 1–3) and the results are consistent with previous data (Philipson *et al.* 2009; Lillehaug *et al.* 2014). MALDI IMS provides the advantage of *in situ* molecular characterization at high chemical specificity, while maintaining the spatial information. For instance, compared to off tissue MS analysis on, e.g. tissue extracts, IMS facilitates peptide signal attribution to small anatomical structures such as individual plaques (Fig. 1).

In the present study we performed imaging MS analysis at 50 μm spatial resolution. However, the laser focus setting (medium) corresponds to a laser spot size of 50–60 μm and the number of shots per pixel (1000) will lead to full matrix ablation. Therefore, slight oversampling might occur. Typically, spatial information on protein and peptide localization *in situ* is obtained through immunohistochemical staining, as demonstrated here for validating the IMS data (Fig. 2). However, immunohistochemical methods do not allow comprehensive molecular analysis of more than 3–4 target species at a time. This limitation has, however, been overcome by combining immunohistochemistry with mass cytometry, i.e. imaging mass cytometry, allowing for potential multiplexed analysis for over 100 target species at once (Giesen *et al.* 2014). Despite its obvious great potential, this technique requires *a priori* knowledge of the targeted species and is dependent on antibody specificity just as regular immunohistochemistry. Therefore, MALDI IMS should be considered a powerful alternative for probing molecular changes *in situ*, such as characterizing Aβ deposition in brain tissue. Indeed, recent studies in Alzheimer's tissue have demonstrated the possibility to detect various Aβ truncations with the help of MALDI IMS (Philipson *et al.* 2012; Kelley *et al.* 2016).

In this study, MALDI IMS analysis revealed region-dependent differences in plaque-associated Aβ peptide composition in three different brain regions in the tgArcSwe mice, as obtained by spectral data analysis of individual deposits using SAM-based multivariate analysis with paired *t* statistics (Figs. 4 and 5). The data show significant

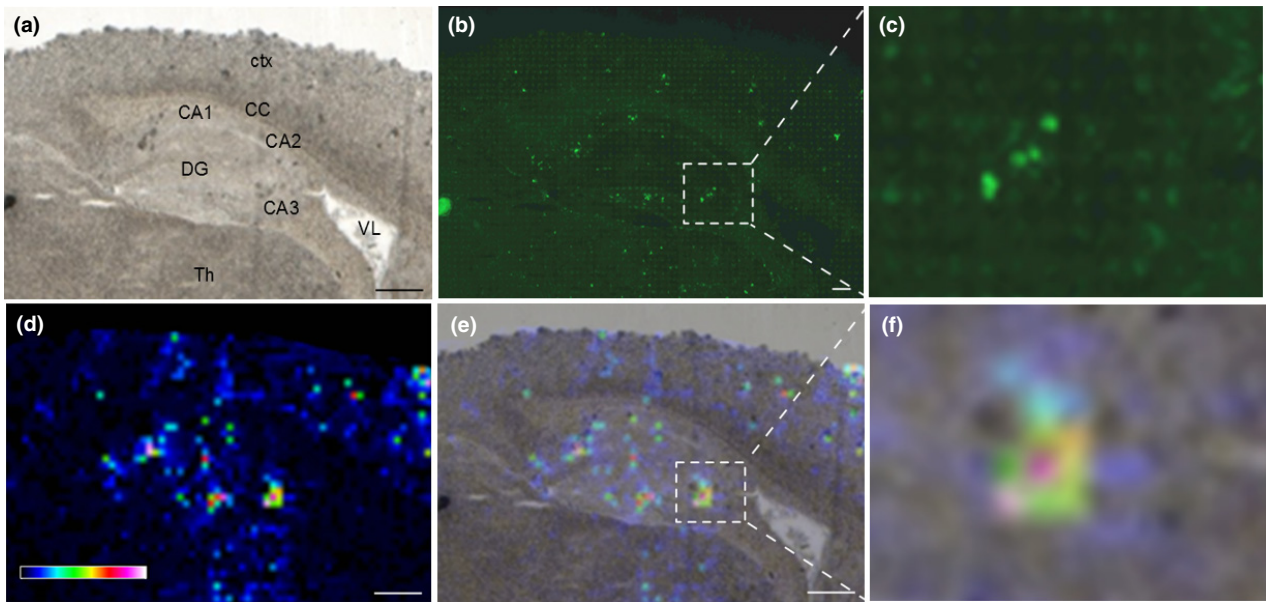

Fig. 2 Identification of Aβ deposits localized with matrix-assisted laser desorption/ionization (MALDI) imaging mass spectrometry (IMS) using immunohistochemistry. (a) Wide field micrograph showing an overview of substructures in the hippocampal and cortical regions; ctx = cerebral cortex, cc = corpus callosum, CA1, CA2 and CA3 = hippocampal subregions (cornu Ammonis), DG = dentate gyrus, VL = lateral ventricle, Th = thalamus. (b and c) Immunohistochemical fluorescence microscopy images of Aβ deposits stained with monoclonal 6E10 antibody and Alexa Fluor 488 goat anti-mouse secondary antibodies. (d) Single ion image of Aβ(1-40arc) peptides (m/z 4256) using MALDI IMS. (e–f) Overlay of (d) and (a) reveals Aβ structures in the hippocampal and cortical regions. The magnified images of immunostained Aβ deposits (c) and MALDI IMS ion image [Aβ(1-40arc)] (f) from same area [illustrated by the squares in (b) and (e)] verifies co-localization of Aβ deposits. Scale bars A, D, E = 1 mm, B = 200 μm.

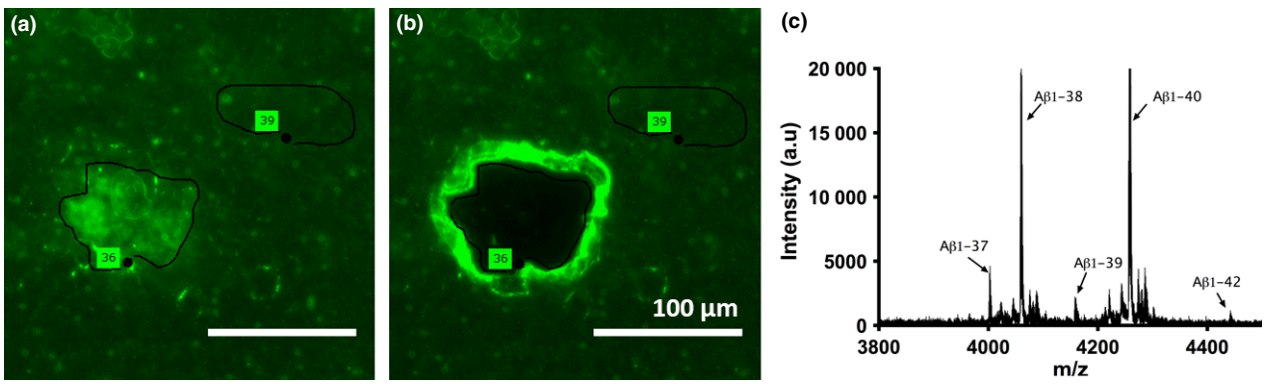

Fig. 3 Laser microdissection and MS analysis of individual Aβ deposits. (a) Histologically identified plaque, stained with heptameric formyl thiophene acetic acids (h-FTAA), and control area of similar size were outlined. (b) Same tissue area after microdissection of the plaque. (c) Matrix-assisted laser desorption/ionization (MALDI) MS data of the plaque extract, confirming the presence of a variety of Aβ peptides in the plaques. Scale bars = 100 μm.

accumulation of the Aβ1-38 and Aβ1-40 species to the plaques, as compared to the surrounding tissue. Similarly, Aβ1-42 was found to localize to the deposits in the hippocampus and the somatosensory cortex (SS), suggesting that Aβ1-42 is predominantly associated with extracellular plaques in these brain regions.

In contrast, the somatomotor-associated cortex (MO) displayed a more disperse Aβ1-42 distribution without a significant enrichment to the plaques. This non-plaque specific, disperse distribution points towards a high degree of soluble intra- and extra-neuronal accumulation of Aβ1-42 resulting in high signal within the control area at 18 months. Results reported in a previous time course study on tgArcSwe mice at different ages suggest that an accumulation of soluble Aβ42 takes place only up to a certain level, after which the concentration is decreased as a result of

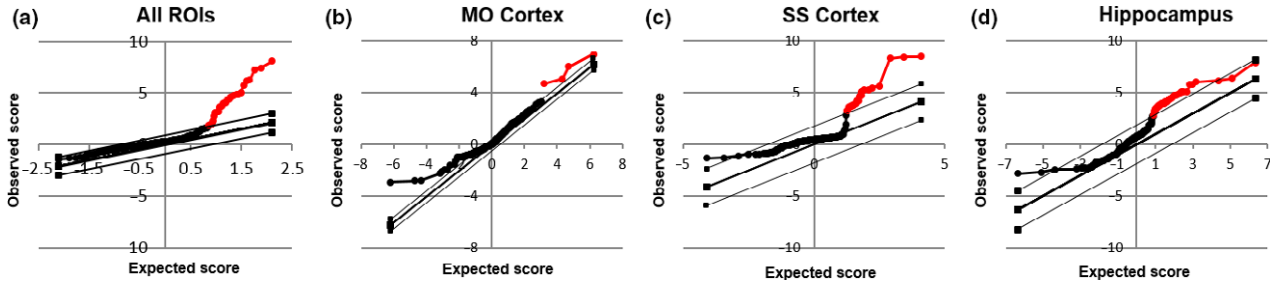

Fig. 4 Statistical analysis of peak intensity differences between plaques and adjacent control areas. Two-class, paired analysis was performed using SAM in (a) the pooled data from all three brain regions, (b) the somatomotor cortex (MO), (c) the somatosensory cortex (SS) and (d) hippocampus. The graphs depict for each variable (peak m/z value) the observed SAM score, indicating the relative difference between control and plaque. The expected score indicates the random fluctuation when there is no difference in between the two groups. Red marked variables indicate m/z values that are increased in the plaque compared to the control, where the difference of the observed (SAM) versus the expected score is above a certain threshold (indicated by thin lines), representing the 95% significance level.

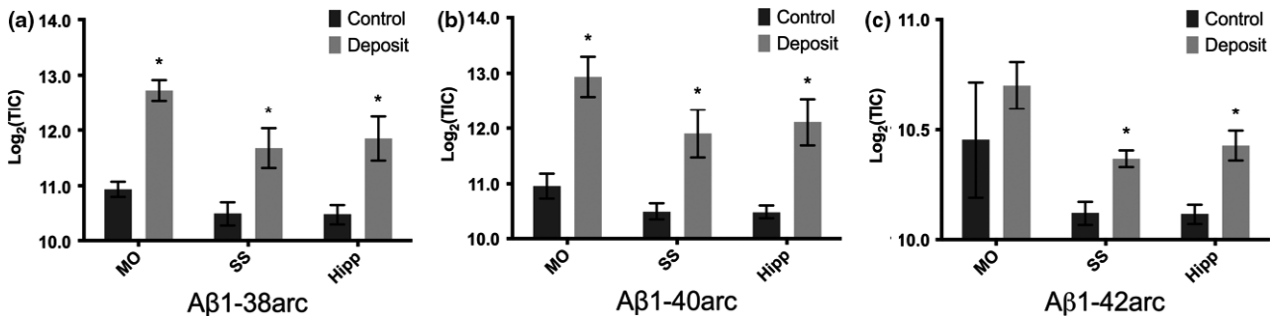

Fig. 5 Statistical analysis of the Aβ content in the three studied regions of the mouse brain: the somatomotor cortex (MO), somatosensory cortex (SS) and hippocampus (Hipp). Individual Aβ deposits were compared with adjacent control regions within the same tissue section. Two peptides: (a) Aβ(1-38) and (b) Aβ(1-40) were found to be elevated in the deposits as compared to the control areas in all three regions. (c) The signal of Aβ(1-42) was found to be significantly increased in the somatosensory cortex and hippocampus, but not in the somatomotor cortex (mean ± SEM, $n = 3$, $p < 0.05$). *p < 0.05

extracellular Aβ42 aggregation into amyloid plaques. This and other studies demonstrate an increase of Aβ42 in extracellular Aβ deposits with age in both the hippocampus and cortex as assessed by immunohistochemistry using Aβ42-specific antibodies (Lord *et al.* 2006; Philipson *et al.* 2009). Hence, a disperse, non-significant localization of Aβ1-42 signal to plaques in somatomotor cortex as observed in the present study could indicate a continued non-plaque-specific accumulation of extracellular Aβ1-42 in this region, predating plaque pathology. Alternatively, the chemical composition of the hippocampal and somatosensory cortical plaques might be different compared to plaques in the somatomotor-associated cortex. While the MS imaging data in the current study on 18-month-old tgArcSwe mice provide further insight into Aβ aggregation pathology, further more comprehensive neuropathological study of tgArcSwe mice, including a long-term, time-resolved study of age-dependent changes in plaque pathology is needed.

Our analysis of individual Aβ deposits and adjacent control regions revealed increased concentrations of macrophage migration inhibitory factor (MIF) and other unknown proteins in the vicinity of the plaques. Here, the identity and localization of MIF was verified by immunohistochemistry (Fig. 6). It was furthermore demonstrated that MIF localizes specifically to hippocampal amyloid plaques. MIF is a proinflammatory cytokine expressed in microglia and is considered to play an important role in brain inflammatory processes (Metz and Bucala 1997; Bacher *et al.* 1998). Indeed immunohistochemical co-staining toward Iba1, a marker for microglia activation, MIF and Aβ revealed a high degree of co-localization of plaque-associated MIF with Iba1 (Fig. 6f). This suggests a high degree of microglial activation, which is suggested to be an important factor in AD pathology. Indeed, elevated levels of MIF in cerebral spinal fluid have been reported in AD patients (Bacher *et al.* 2010). Although MIF has been implicated in AD pathology, its relevance beyond proinflammatory response is not fully understood. It has been found that MIF can form amyloid-like structures and interact with Aβ, as shown by studies of immunoprecipitates in soluble fractions of AD brain (Lashuel *et al.* 2005). The binding of MIF to Aβ has been suggested to play a crucial role in the accumulation of Aβ into senile

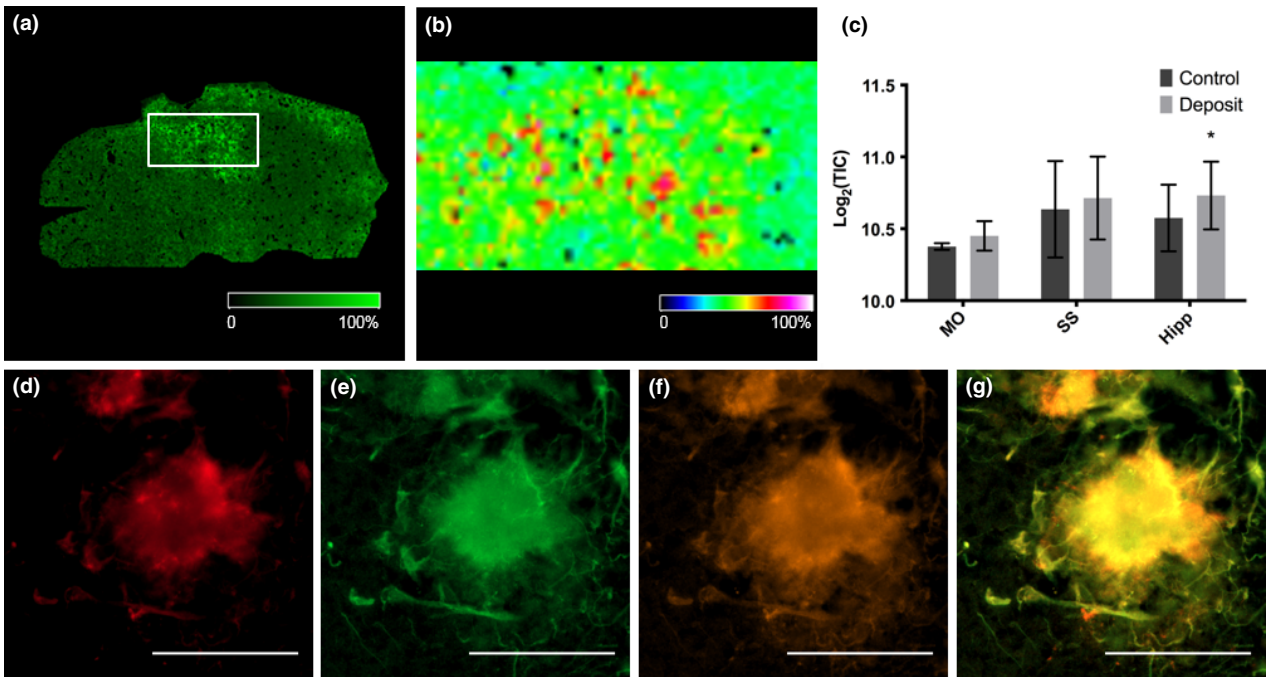

Fig. 6 Identification and localization of macrophage migration inhibitory factor (MIF) with matrix-assisted laser desorption/ionization (MALDI) imaging mass spectrometry (IMS) and confirmation with immunohistochemistry. (a and b) MALDI image of the hippocampal region (Hipp) for ion peak at m/z 6175, putatively assigned to MIF. (c) MIF localization to Aβ deposits as compared with adjacent control area within different regions of the same tissue section. Signal attributed to MIF was shown to be significantly increased only in hippocampus (Hipp, mean ± SEM, $n = 3$, $p < 0.05$) but not in the somatomotor (MO) and somatosensory (SS)-associated cortex. (d) Immunohistochemical labeling of Aβ deposits with monoclonal 6E10 antibody, (e) polyclonal anti-MIF antibody and (f) polyclonal anti-Iba1 antibody. (g) Overlay image of Aβ deposits (red), MIF (green) and Iba1 (orange) shows clear co-localization in the hippocampal region of the brain. Scale bar = 50 μm.

plaques, although co-localization of MIF and Aβ has been observed only to a varying degree (Oyama *et al.* 2000; Lashuel *et al.* 2005; Bacher *et al.* 2010). Previous studies of tg2576 mice, a transgenic AD model with only the Swedish mutation, failed to demonstrate such co-localization of MIF to the Aβ deposits (Lashuel *et al.* 2005). In contrast, immunohistochemical staining in APP23 mice, another transgenic AD model that also expresses the Swedish mutation, showed distinct MIF staining in proximity to the plaques (Bacher *et al.* 2010). This suggests that the enhanced distribution of MIF to Aβ deposits in transgenic mouse brains is highly dependent on the model that is used, as well as on the structure of the Aβ plaque and on the anatomical brain region of the Aβ deposition. Indeed, the APP23 model is similar to the tgArcSwe model in that the observed plaque phenotype resembles more compact, dense core plaques as observed in human brain tissue (Lord *et al.* 2006; Philipson *et al.* 2010). This in turn suggests a link between the morphological plaque phenotype and increased MIF accumulation to these plaques.

Conclusions

The present study demonstrates the potential of MALDI imaging as a powerful technique for elucidating changes in the spatial distributions of proteins and peptides associated with pathological mechanisms in Alzheimer's disease. Multivariate statistical analysis of the imaging MS data and subsequent spectral data analysis of individual amyloid deposits revealed significant differences in the protein/peptide composition of deposits located in different anatomical regions of the brain, including different Aβ peptides and other plaque-associated proteins. Furthermore, a distinct accumulation of macrophage migration inhibitory factor (MIF) was observed to the plaques, suggesting that neuroinflammatory processes and glial cell reactivity is involved in the AD pathology. The presented data further highlight the potential of IMS as a powerful approach in neuropathology.

Acknowledgments and conflict of interest disclosure

The Swedish Research Council VR (#2014-6447, JH; #2015-04199, PS; #2012-1593, SS), the Royal Society of Arts and Sciences in Gothenburg (KVVS, JH), Alzheimerfonden (JH, SS), Demensfonden (JH), Jeanssons Stiftelsen (JH), Ahlén Stiftelsen (JH, SS), Stiftelsen Gamla Tjänarinnor (JH), Stohnes Stiftelse (JH, SS) and Stiftelsen Wilhelm och Martina Lundgrens Vetenskapsfond (JH) are acknowledged for financial support. We would also like to thank

Prof Lars N. Nilsson who developed the mouse model as well as Prof Lars Lannfelt for critically reading the manuscript. The authors declare no conflict of interest.

All experiments were conducted in compliance with the ARRIVE guidelines.

References

Altelaar A. F. A., Taban I. M., McDonnell L. A., Verhaert P. D. E. M., de Lange R. P. J., Adan R. A. H., Mooi W. J., Heeren R. M. and Piersma S. R. (2007) High-resolution MALDI imaging mass spectrometry allows localization of peptide distributions at cellular length scales in pituitary tissue sections. *Int. J. Mass Spectrom.* **260**, 203–211.

Arriagada P. V., Growdon J. H., Hedley-Whyte E. T. and Hyman B. T. (1992) Neurofibrillary tangles but not senile plaques parallel duration and severity of Alzheimer's disease. *Neurology* **42**, 631–639.

Bacher M., Meinhardt A., Lan H. Y. *et al.* (1998) MIF expression in the rat brain: implications for neuronal function. *Mol. Med.* **4**, 217–230.

Bacher M., Deuster O., Aljabari B. *et al.* (2010) The role of macrophage migration inhibitory factor in Alzheimer's disease. *Mol. Med.* **16**, 116–121.

Ballard C., Gauthier S., Corbett A., Brayne C., Aarsland D. and Jones E. (2011) Alzheimer's disease. *The Lancet* **377**, 1019–1031.

Braak H. and Braak E. (1991) Neuropathological staging of Alzheimer-related changes. *Acta Neuropathol.* **82**, 239–259.

Caprioli R. M., Farmer T. B. and Gile J. (1997) Molecular imaging of biological samples: localization of peptides and proteins using MALDI-TOF MS. *Anal. Chem.* **69**, 4751–4760.

van Duijn C. M., Hendriks L., Cruts M., Hardy J. A., Hofman A. and Van Broeckhoven C. (1991) Amyloid precursor protein gene mutation in early-onset Alzheimer's disease. *Lancet* **337**, 978.

Giesen C., Wang H. A., Schapiro D. *et al.* (2014) Highly multiplexed imaging of tumor tissues with subcellular resolution by mass cytometry. *Nat. Methods* **11**, 417–422.

Hanrieder J., Ljungdahl A., Falth M., Mammo S. E., Bergquist J. and Andersson M. (2011a) L-DOPA-induced dyskinesia is associated with regional increase of striatal dynorphin peptides as elucidated by imaging mass spectrometry. *Mol. Cell Proteomics* **10**(M111), 009308.

Hanrieder J., Wicher G., Bergquist J., Andersson M. and Fex-Svenningsen Å. (2011b) MALDI mass spectrometry based molecular phenotyping of CNS glial cells for prediction in mammalian brain tissue. *Anal. Bioanal. Chem.* **401**, 135–147.

Hanrieder J., Phan N. T. N., Kurczy M. E. and Ewing A. G. (2013) Imaging mass spectrometry in neuroscience. *ACS Chemical Neuroscience* **4**, 666–679.

Hardy J. A. and Higgins G. A. (1992) Alzheimer's disease: the amyloid cascade hypothesis. *Science* **256**, 184–185.

Hardy J. and Selkoe D. J. (2002) Medicine - The amyloid hypothesis of Alzheimer's disease: progress and problems on the road to therapeutics. *Science* **297**, 353–356.

Kelley A. R., Perry G., Castellani R. J. and Bach S. B. (2016) Laser-induced in-source decay applied to the determination of amyloid-beta in Alzheimer's brains. *ACS Chem Neurosci*, **7**, 261–268.

Lashuel H. A., Aljabari B., Sigurdsson E. M., Metz C. N., Leng L., Callaway D. J. and Bucala R. (2005) Amyloid fibril formation by macrophage migration inhibitory factor. *Biochem. Biophys. Res. Commun.* **338**, 973–980.

Lillehaug S., Syverstad G. H., Nilsson L. N., Bjaalie J. G., Leergaard T. B. and Torp R. (2014) Brainwide distribution and variance of amyloid-beta deposits in tg-ArcSwe mice. *Neurobiol. Aging* **35**, 556–564.

Lord A., Kalimo H., Eckman C., Zhang X.-Q., Lannfelt L. and Nilsson L. N. G. (2006) The Arctic Alzheimer mutation facilitates early intraneuronal Aβ aggregation and senile plaque formation in transgenic mice. *Neurobiol. Aging* **27**, 67–77.

Martin Prince A. W., Maëlenn G., Gemma-Claire A., Yu-Tzu W. and Matthew P. (2015) World Alzheimer Report 2015: The Global Impact of Dementia - An analysis of prevalence, incidence, cost and trends. http://www.alz.co.uk/research/world-report-2015.

McDonnell L. A. and Heeren R. M. A. (2007) Imaging mass spectrometry. *Mass Spectrom. Rev.* **26**, 606–643.

Metz C. N. and Bucala R. (1997) Role of macrophage migration inhibitory factor in the regulation of the immune response. *Adv. Immunol.* **66**, 197–223.

Nilsberth C., Westlind-Danielsson A., Eckman C. B. *et al.* (2001) The 'Arctic' APP mutation (E693G) causes Alzheimer's disease by enhanced A[beta] protofibril formation. *Nat. Neurosci.* **4**, 887–893.

Oyama R., Yamamoto H. and Titani K. (2000) Glutamine synthetase, hemoglobin alpha-chain, and macrophage migration inhibitory factor binding to amyloid beta-protein: their identification in rat brain by a novel affinity chromatography and in Alzheimer's disease brain by immunoprecipitation. *Biochim. Biophys. Acta* **1479**, 91–102.

Philipson O., Hammarstrom P., Nilsson K. P. *et al.* (2009) A highly insoluble state of Abeta similar to that of Alzheimer's disease brain is found in Arctic APP transgenic mice. *Neurobiol. Aging* **30**, 1393–1405.

Philipson O., Lord A., Gumucio A., O'Callaghan P., Lannfelt L. and Nilsson L. N. (2010) Animal models of amyloid-β-related pathologies in Alzheimer's disease. *FEBS J.* **277**, 1389–1409.

Philipson O., Lord A., Lalowski M. *et al.* (2012) The Arctic amyloid-ß precursor protein (AßPP) mutation results in distinct plaques and accumulation of N- and C-truncated Aß. *Neurobiol. Aging*, **33**, 1010.e1011-1010.e1013.

Portelius E., Bogdanovic N., Gustavsson M. K., Volkmann I., Brinkmalm G., Zetterberg H., Winblad B. and Blennow K. (2010) Mass spectrometric characterization of brain amyloid beta isoform signatures in familial and sporadic Alzheimer's disease. *Acta Neuropathol.* **120**, 185–193.

Rahman S. M., Gonzalez A. L., Li M. *et al.* (2011) Lung cancer diagnosis from proteomic analysis of preinvasive lesions. *Cancer Res.* **71**, 3009–3017.

Rohner T. C., Staab D. and Stoeckli M. (2005) MALDI mass spectrometric imaging of biological tissue sections. *Mech. Ageing Dev.* **126**, 177–185.

Schaeffer E. L., Figueiro M. and Gattaz W. F. (2011) Insights into Alzheimer disease pathogenesis from studies in transgenic animal models. *Clinics* **66**, 45–54.

Stoeckli M., Staab D., Staufenbiel M., Wiederhold K.-H. and Signor L. (2002) Molecular imaging of amyloid β peptides in mouse brain sections using mass spectrometry. *Anal. Biochem.* **311**, 33–39.

Tekirian T. L. (2001) Commentary: Abeta N- Terminal Isoforms: critical contributors in the course of AD pathophysiology. *J. Alzheimers Dis.* **3**, 241–248.

Tusher V. G., Tibshirani R. and Chu G. (2001) Significance analysis of microarrays applied to the ionizing radiation response. *Proc. Natl Acad. Sci. USA* **98**, 5116–5121.